

Current profile control by alternating current magnetic helicity injection

F. Ebrahimi and S. C. Prager

University of Wisconsin—Madison, Madison, Wisconsin 53706

(Received 29 December 2003; accepted 4 February 2004; published online 15 April 2004)

Current profile control by ac magnetic helicity injection is computationally investigated in a reversed field pinch (RFP). Three-dimensional resistive magnetohydrodynamics (MHD) computation is employed to study the nonlinear MHD. During ac helicity injection, when toroidal and poloidal surface voltages are oscillated out of phase, the parallel electric field is maintained positive over a majority of the cycle leading to current density profile flattening. The total time-averaged magnetic fluctuations are reduced and the magnetic surfaces are nonstochastic for much of the cycle. The steady-state nature of this technique could make it useful for improving RFP performance. © 2004 American Institute of Physics. [DOI: 10.1063/1.1690304]

I. INTRODUCTION

In the conventional reversed field pinch (RFP) configuration, the plasma current is driven and sustained by a toroidal inductive electric field. The resulting electric field component parallel to the magnetic field is centrally peaked, leading to a current density profile unstable to tearing modes. Energy confinement is consequently reduced. In recent years, energy confinement has been greatly improved through tearing mode reduction by control of the radial profile of the current density. The technique applied successfully in experiment is control of the inductive current density profile. A surface poloidal inductive electric field has been applied to drive edge poloidal current, which in the RFP edge is mainly in the parallel direction.¹ Most recently, further refinement of the current density profile is obtained by the addition of programming of the toroidal electric field.² Although successful at demonstrating confinement improvement, the technique is limited in its utility since it is transient. Application of a unidirectional poloidal electric field causes the toroidal magnetic flux to decay in time. To circumvent this problem, we investigate here current density profile control by ac magnetic helicity injection—a technique that operates in an oscillatory steady-state.

Oscillating field current drive (OFCD) is a form of ac helicity injection first proposed in the RFP in Ref. 3. In OFCD, poloidal and toroidal surface voltages are oscillated 90 deg out of phase to inject magnetic helicity into the plasma and sustain steady-state current. Recently, we have investigated the three-dimensional (3-D) nonlinear MHD of full current sustainment by OFCD. While OFCD sustains the current, it also leads to the excitation of edge-resonant modes with large amplitudes. The core-resonant tearing modes are not strongly affected.⁴ Here we computationally study OFCD for the different purpose of current density profile control. Although a portion of the total current is sustained steadily, the key effect of interest is the reduction of magnetic fluctuations.

Using the concept of magnetic helicity balance, the rate of change of magnetic helicity is

$$\frac{\partial K}{\partial t} = 2(\phi_z v_z) - 2 \int \mathbf{E} \cdot \mathbf{B} dv, \quad (1)$$

where magnetic helicity, a measure of the knottedness of the magnetic field lines, is defined as $K = \int \mathbf{A} \cdot \mathbf{B} dv - \phi_p \phi_z$, ϕ_p is the poloidal flux passing through the center of the torus, ϕ_z is the axial flux within the plasma, and v_z is the loop voltage.^{5,6} For OFCD, the helicity injection rate $\phi_z v_z$ on the RHS of Eq. (1) consists of the contribution from both the ohmic helicity injection rate $(\phi_z v_z)_{dc}$ and the ac helicity injection rate $\hat{\phi}_z \hat{v}_z$ (the “hat” denotes an oscillating quantity). In steady-state, the dissipation rate (the second term on the RHS) balances the helicity injection rate. Electrostatic helicity injection, which requires the intersection of magnetic field lines with biased electrodes, has been studied earlier and shown to stabilize tearing modes.⁷

The numerical model and the basic equations are presented in Sec. II. In Sec. III the time-averages of both the axisymmetric quantities and the non-axisymmetric fluctuations are presented. The time variations of both axisymmetric fields and the asymmetric magnetic fluctuations throughout an OFCD cycle are discussed in Sec. IV. To understand the dynamics of OFCD for current profile control, we first study oscillating poloidal current drive (OPCD) in which only the poloidal surface electric field is oscillated, then oscillating toroidal current drive (OTCD) in which only the surface toroidal electric field is oscillated. The fluctuation level oscillated in both cases, but the net decrease is minor. OPCD has been enacted in experiment,⁸ with only modest gain in confinement. The detailed dynamics of OPCD and OTCD are presented in Secs. IV A and B. Significant reduction of tearing fluctuations requires the oscillation of both poloidal and toroidal voltages—OFCD. Only then is the parallel electric field profile sufficiently flattened. The dynamics of OFCD are described in Sec. IV C. The ac helicity injection rate decreases with oscillation frequency. However, the frequency should be low enough that edge OFCD-driven current can be relaxed by the tearing fluctuations into the plasma core to result in current modification, but high enough to avoid current reversal. The optimum balance between these two effects is the topic of Sec. V. We conclude in Sec. VI.

II. NUMERICAL MODEL

We study the full dynamics of fluctuation reduction by OFCD with 3-D MHD computations, capable of tracking changes in the tearing fluctuations. The 3-D resistive MHD code, DEBS,⁹ is employed to solve the compressible resistive MHD equations in periodic cylindrical geometry,

$$\begin{aligned} \frac{\partial \mathbf{A}}{\partial t} &= S \mathbf{V} \times \mathbf{B} - \eta \mathbf{J}, \\ \rho \frac{\partial \mathbf{V}}{\partial t} &= -S \rho \mathbf{V} \cdot \nabla \mathbf{V} + S \mathbf{J} \times \mathbf{B} + \nu \nabla^2 \mathbf{V}, \\ \mathbf{B} &= \nabla \times \mathbf{A}, \\ \mathbf{J} &= \nabla \times \mathbf{B}, \end{aligned} \quad (2)$$

where time and radius are normalized to the resistive diffusion time $\tau_R = 4\pi a^2/c^2 \eta_0$ and the minor radius a , velocity to the Alfvén velocity V_A , and magnetic field \mathbf{B} to the magnetic field on axis B_0 . The Lundquist number $S = \tau_R/\tau_A$ (where $\tau_A = a/V_A$), and ν is the viscosity coefficient, which measures the ratio of characteristic viscosity to resistivity (the magnetic Prandtl number). The mass density ρ is assumed to be uniform in space and time. The resistivity profile increases near the plasma edge, $\eta = (1 + 9(r/a)^{20})^2$. Oscillating axial and azimuthal electric fields are imposed at the wall, $\hat{E}_z = \varepsilon_z \sin(\omega t)$, $\hat{E}_\theta = \varepsilon_\theta \sin(\omega t + \pi/2)$, where ε_z and ε_θ are the axial and azimuthal ac amplitudes, respectively. For sufficient relaxation, the oscillation period should be long compared to the plasma relaxation time (the hybrid tearing time scale $\tau_H \sim \sqrt{\tau_R \tau_A}$). To avoid large current modulations, this period should be short compared to resistive diffusion time τ_R ($\tau_H < \tau_\omega < \tau_R$).

To inject ac magnetic helicity, we impose oscillating fields on a relaxed plasma (standard RFP) which is ohmically sustained by an axial time-independent electric field. In the present simulations about 50% of the dc magnetic helicity (ohmic helicity) is injected by oscillating fields. The computations are at Lundquist number $S = 10^5$, magnetic Prandtl number $Pm = 10$, and aspect ratios $R/a = 2.88$ (MST aspect ratio) and $R/a = 1.66$. For high aspect ratio $R/a = 2.88$, we have used resolution of 220 radial mesh points, 41 axial modes ($-41 < n < 41$), and 5 azimuthal modes ($0 \leq m < 5$). Lower resolution is sufficient for aspect ratio $R/a = 1.66$.

III. TIME-AVERAGED QUANTITIES

To form the initial standard RFP plasma, the computations are started with a specified time-independent axial electric field at the wall, $E_z(r=1)$. In the standard RFP simulations, the nonlinear resistive MHD equations are evolved with nonzero initial asymmetric fluctuations which affect the axisymmetric profiles. The resulting parallel electric field is peaked in the plasma core and generates a current profile which is linearly unstable against current-driven resistive MHD instabilities. The resulting tearing fluctuations grow and through nonlinear mode coupling a quasi stationary-state relaxed RFP plasma is formed. The tearing fluctuations distribute the plasma current through the dynamo process. The

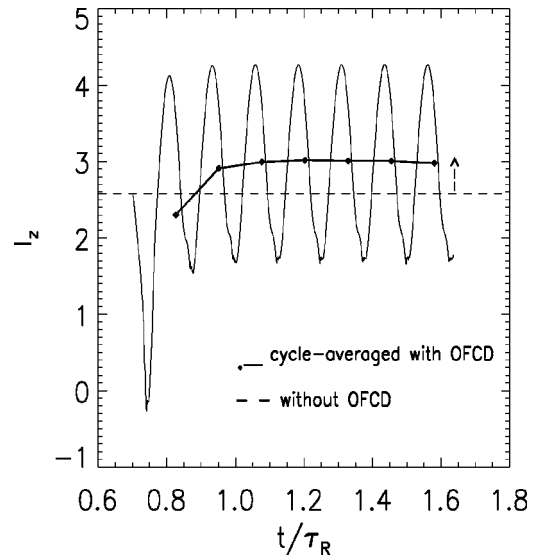


FIG. 1. Total axial current with partial OFCD at the frequency $\omega\tau_H = 0.16$ versus time. The cycle-averaged current with OFCD (line with diamonds) shows about 15% boost. The dashed line shows the current without OFCD (standard).

initial target RFP plasma used in the simulations presented in this section has a pinch parameter $\Theta = 1.68$, where $\Theta = I_z/2\phi_z$, at aspect ratio $R/a = 1.66$. The oscillating fields are then imposed on the target relaxed RFP plasma.

The ac helicity injection rate, $\dot{K}_{inj} = \hat{v}_z \hat{v}_\theta / 2\omega = 19$, is about 50%–60% that of the ohmic dc helicity. We choose an OFCD frequency $\omega\tau_H = 0.16$ ($\tau_\omega = 12000\tau_A$), which is low enough for both the relaxation and modification of the current density. The total axial current is shown in Fig. 1. Because of the low frequency, the modulation amplitudes for this case are large (about 75% of the mean). The time-averaged (over an OFCD period) total axial current is increased by 10%–15%.

The cycle-averaged parallel current density is increased as shown in Fig. 2(a). The modification of the cycle-averaged $\lambda = J_\parallel/B$ profile with the partial OFCD can be seen in Fig. 2(b). OFCD makes the λ profile flatter around $r \approx 0.8$ with the reduction of the gradient starting at $r \approx 0.5$.

The dynamics of current sustainment can be investigated using the cycle-averaged Ohm's law,

$$\bar{\mathbf{E}}_\parallel + \overline{(\mathbf{V}_{00} \times \mathbf{B}_{00})_\parallel} + \langle \tilde{\mathbf{V}} \times \tilde{\mathbf{B}} \rangle_\parallel = \overline{\eta \mathbf{J}_\parallel}, \quad (3)$$

where \mathbf{V}_{00} and \mathbf{B}_{00} are the oscillating velocity and magnetic fields with poloidal and toroidal mode numbers $m = n = 0$, $\tilde{\mathbf{V}}$ and $\tilde{\mathbf{B}}$ are the fields with $m, n \neq 0$, and $\langle \rangle$ denotes an average over a magnetic surface [$(\cdot)_\parallel = (\cdot) \cdot \bar{\mathbf{B}}/B$, where $\bar{\mathbf{B}}$ is the cycle-averaged mean (0,0) magnetic field]. The over-bar indicates a time-average (i.e., cycle-average) value. The second and third terms are the dynamo terms generated by the axisymmetric oscillations and the non-axisymmetric tearing instabilities, respectively. The first term $\bar{\mathbf{E}}_\parallel$ is the ohmic toroidal electric field which is zero for the full current sustainment by OFCD in the absence of a dc loop voltage.⁴ The second term is the OFCD dynamo, current driven directly by

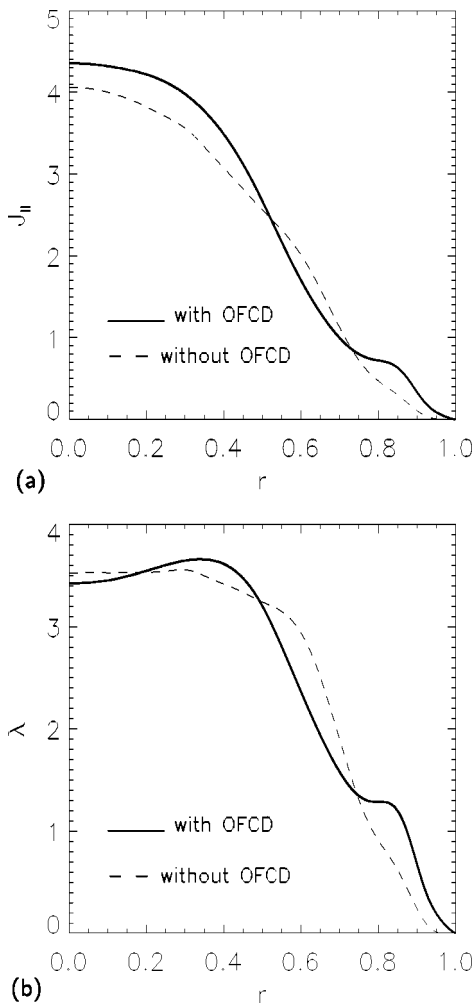


FIG. 2. Radial profiles of the cycle-averaged (a) parallel current density $J_{||}$ and (b) the $\lambda = J_{||}/B$ profiles. The dashed lines denote the same profiles for standard RFP (without OFCD).

the OFCD fields. Using $\mathbf{V}_{00} = \mathbf{E}_{00} \times \bar{\mathbf{B}}/B^2$, the first and second terms can be combined and written as $(\mathbf{E}_{00} \cdot \mathbf{B}_{00})/B$. Therefore, we can consider the first two terms on the LHS of Eq. (3) as the time-averaged parallel component of electric field which has both dc and oscillating (ac) components. We see that the cycle-averaged parallel current is sustained by all the three terms on the LHS of Eq. (3). However, as we will discuss in more detail later, the time variation of the current density profile during a cycle is substantial. The cyclic variations of the electric field and the resulting parallel current gradients affect the resistive MHD instabilities and the tearing fluctuation amplitudes. Thus, the significant effect is the reduction of the total fluctuation amplitudes. As it is shown in Fig. 3 the fluctuation amplitude becomes zero during part of the OFCD cycle. The time-average of the total rms fluctuation amplitudes decreases by a factor of 2–2.5. Below we present the detailed analysis of this case during a cycle.

IV. TIME DEPENDENCE

A salient feature of OFCD sustainment is the large variation of the axisymmetric profiles during a cycle. As shown above, large oscillations of the total axial current are ob-

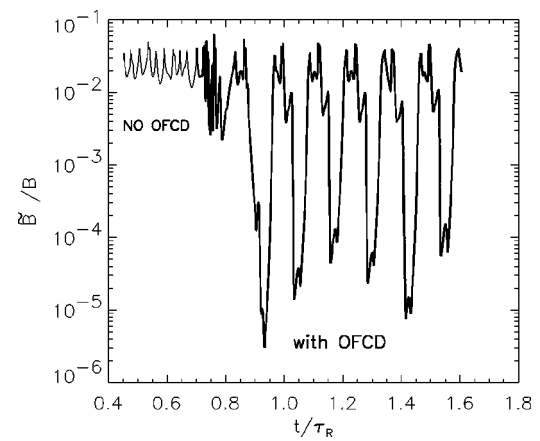


FIG. 3. The radial component of the magnetic fluctuation amplitude [$\text{rms}(\tilde{B}/B)$] with and without OFCD.

served. The axisymmetric magnetic and velocity fields also exhibit large variations. Therefore, in this section we study the detailed dynamics of profile variations and magnetic fluctuations throughout a cycle. The time-averaged magnetic fluctuations exhibit a reduction by a factor of 2 by applying OFCD. The physics behind the modified current profile and the suppression of the magnetic fluctuations can be explained in part through detailed study of the profile variations of the three terms in parallel Ohm's law: the current density, the electric field and the fluctuation-induced dynamo terms.

To elucidate the ingredients of OFCD for current profile control, we first investigate oscillating poloidal current drive (OPCD) and oscillating toroidal current drive (OTCD) separately. We study the separate effect of OPCD and OTCD on both current profile and magnetic fluctuations. Then, we present the OFCD dynamics in which both toroidal and poloidal electric fields are oscillated out of phase to inject a time-averaged magnetic helicity and to modify the current profile.

A. Oscillating poloidal current drive (OPCD)

An oscillating poloidal electric field ($\hat{E}_\theta = \varepsilon_\theta \sin(\omega t + \pi/2)$, $\varepsilon_\theta = 2.4$, $\tau_\omega = 0.126\tau_R$) is imposed at the plasma wall on a target standard plasma at time $t = 0.7\tau_R$. The poloidal electric field oscillates around a mean zero value, causing the parallel electric field to become both positive and negative during a cycle. This is different from the pulsed poloidal current drive (PPCD) technique for current profile control in which the parallel electric field is experimentally programmed to always remain positive. The radial component of the total magnetic fluctuations \tilde{B}/B and field reversal parameter F are shown in Fig. 4. As it is seen, the total magnetic fluctuation oscillates with the driving frequency. During part of the cycle, the magnetic fluctuation level is higher than the standard case, while it is lower during the other part of the cycle [see Fig. 4(a)]. Thus, the time-averaged magnetic fluctuation level remains roughly unchanged. Since the frequency is low, the modulation amplitude of the symmetric quantities is large, as seen for the F [Fig. 4(b)]. Mean helicity is not injected by the oscillating poloidal electric field

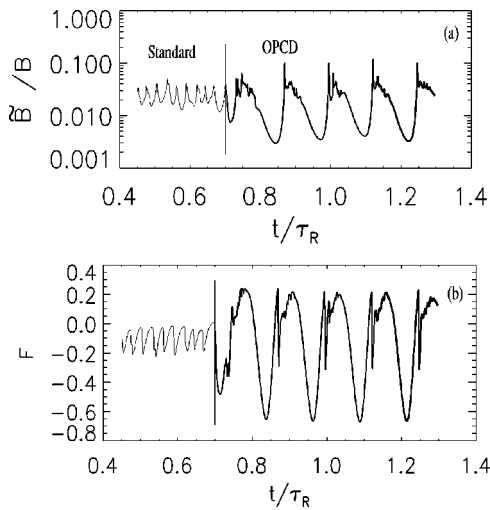


FIG. 4. (a) Radial component of the total magnetic field fluctuations \bar{B}/B . (b) Field reversal parameter, F . At time $t=0.7\tau_R$ an oscillating poloidal field is imposed on a standard plasma. The period of the poloidal electric field is $\tau_\omega=0.126\tau_R$.

($\hat{K}_{OPCD} = \hat{\phi}_z \hat{v}_z = 0$); however, because of the change of the axisymmetric profiles and the reduction of helicity dissipation, there is a slight increase in the time-averaged axial current and helicity. The time-averaged parallel current density J_{\parallel} and $\lambda(r) = J_{\parallel}/B$ profiles are shown in Fig. 5, indicating that the total current does not change significantly (a small amount of current is driven near the plasma edge and the current on axis is reduced). However, the current density gradient is reduced with OPCD from $r=0.6$ to the plasma edge.

Although, the time-averaged effect of the oscillating poloidal electric field on both axisymmetric and asymmetric

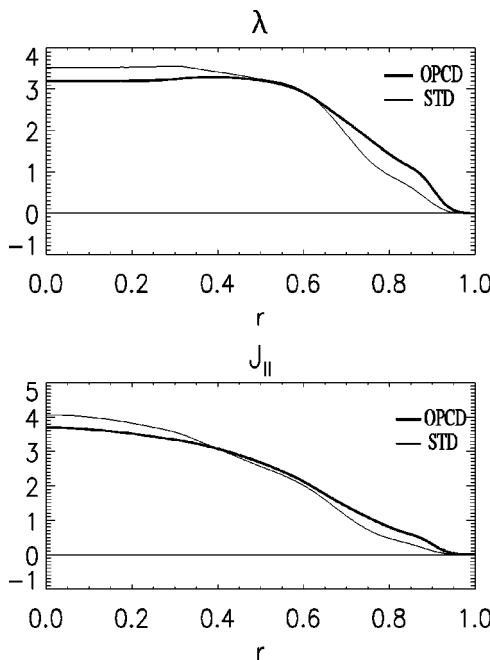


FIG. 5. Time-averaged $\lambda(r)$ and J_{\parallel} profiles for OPCD and standard (STD) cases.

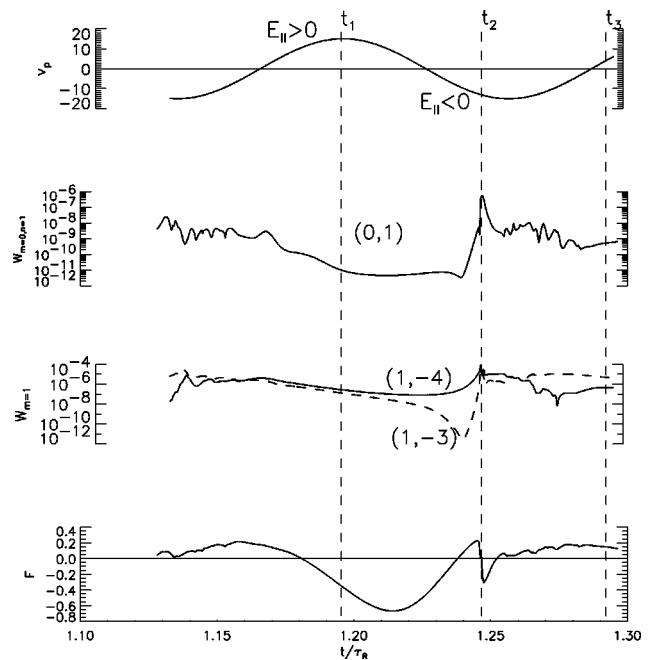


FIG. 6. Oscillating poloidal loop voltage v_p , magnetic modal energy $W_{m,n} = 1/2 \int B_{r,(m,n)}^2 d^3r$ for the (0,1) mode and the core modes (1,-3), (1,-4) and field reversal parameter F versus time.

fields is insignificant, OPCD does affect the radial profiles during a cycle. Figure 6 shows the temporal variations of the modal magnetic energies (W_{mn}), poloidal loop voltage (v_p) and F . It is seen that the core mode magnetic fluctuations are reduced during the positive phase of poloidal electric field ($v_p > 0$) and enhanced during the negative phase ($v_p < 0$). The cause of the fluctuation behavior is revealed by observing the three terms in parallel Ohm's law at three times during a cycle (Fig. 7). The parallel electric field ($E_{\parallel} = E_z \cdot B_z + E_{\theta} \cdot B_{\theta}$) is positive everywhere at time t_1 (while $v_p > 0$, $F < 0$) and a more stable current density profile with smaller gradient is formed [Fig. 7(a)]. The current is sustained by the positive field ($\langle \tilde{V} \times \tilde{B} \rangle_{\parallel} = 0$). Because the magnetic field is mainly poloidal near the edge, during the negative phase with $v_p < 0$ (at t_2), the parallel electric field becomes peaked in the core and negative near the plasma edge [see Fig. 7(b)]. Thus, the current density gradient becomes large which leads to the growth of core resonant modes [(1,-4), (1,-3)] shown in Fig. 6 for t_2 . The dynamo term becomes large (both in the core and at the edge) to relax the unstable current density profile at t_2 [see Fig. 7(b)]. As the poloidal loop voltage changes sign, a positive parallel electric field and consequently positive current density is generated over the entire plasma radius as seen in Fig. 7(c). The positive poloidal electric field modifies the current density profile. As a result the tearing fluctuations are reduced and the cycle repeats. The modification of the λ profile is shown in Fig. 8. The λ profile is flattened in the core at t_1 during the positive phase (edge drive phase $v_p > 0$) and has larger gradient during the negative phase (edge counter-current drive phase $v_p < 0$).

Figure 9 illustrates the variation of the q profile for the three times. The modal magnetic energies shown in Fig. 10

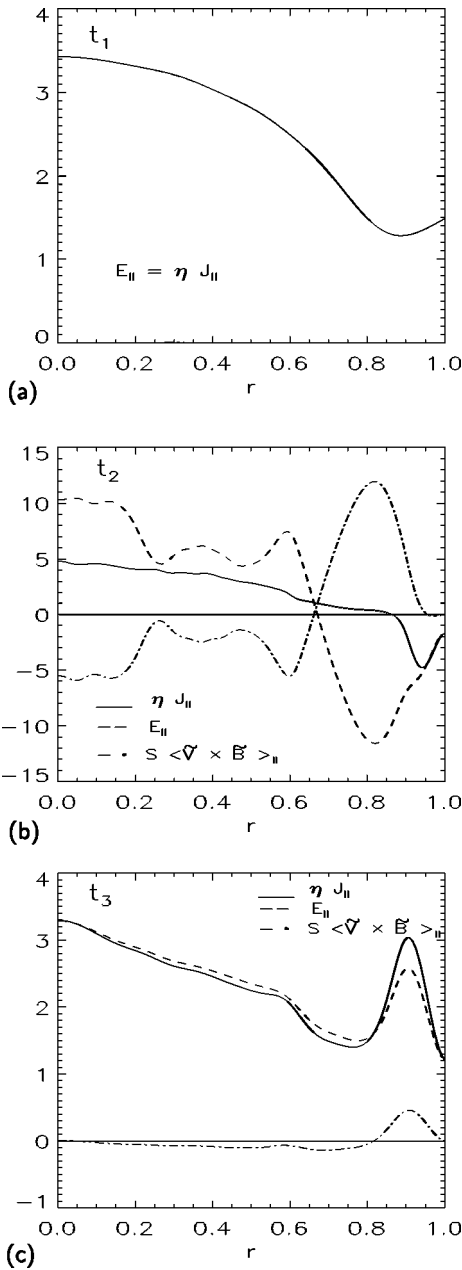


FIG. 7. The three terms in parallel Ohm's law at times (a) t_1 , (b) t_2 , and (c) t_3 for OPCD.

oscillate with the driving frequency and have large modulations, but the time-averaged modal energies are comparable to the standard modal energies. The temporal variations of the total magnetic fluctuations is mainly in phase with variations of the core modal energies $[(1,-3),(1,-4)]$, and the $m=0$ mode nonlinear growth follows after the rapid growth of the dominant core modes (Fig. 10). We conclude that OPCD drives an edge current during the positive phase with $v_p > 0$ and suppresses the magnetic fluctuations, while it generates a counter-current near the edge during the negative phase with $v_p < 0$ and enhances core modal amplitudes.

B. Oscillating toroidal current drive (OTCD)

For OTCD, an oscillating axial electric field $[\hat{E}_z = \varepsilon_z \sin(\omega t), \varepsilon_z = 15]$ is imposed on the plasma wall with the

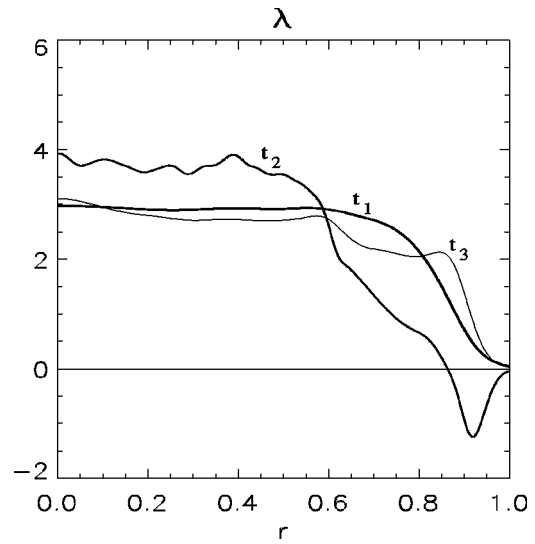


FIG. 8. The $\lambda(r)$ profile during the edge co-current drive phase (t_1 and t_3) and edge counter-current drive phase (t_2) for OPCD.

same initial conditions as for the OPCD case presented above. The axial electric field oscillates with large modulations; its time-averaged value is the standard axial electric field (loop voltage). During the part of the cycle with large negative electric field, the axial current decreases and the fluctuation amplitude increases. Since the axial flux is time-independent ($\hat{E}_\theta = 0$), OTCD does not inject mean helicity ($\overline{K}_{OTCD} = \hat{\phi}_z \hat{v}_z = 0, \hat{\phi}_z = 0$) and consequently does not drive mean current. However, the time-averaged helicity and axial current are reduced with OTCD as shown in Table I. The time-averaged parallel current density J_{\parallel} and $\lambda(r)$ are reduced in the plasma core as shown in Fig. 11.

The time-dependent axial electric field at the boundary causes a large variation in the current profile and magnetic fluctuations. The temporal behavior of F , \tilde{B}/B , and v_z are shown in Fig. 12. The modal magnetic energies, $W_{m,n} = 1/2 \int B_{r,(m,n)}^2 d^3r$, for the core modes $(1,-3)$, $(1,-4)$ and

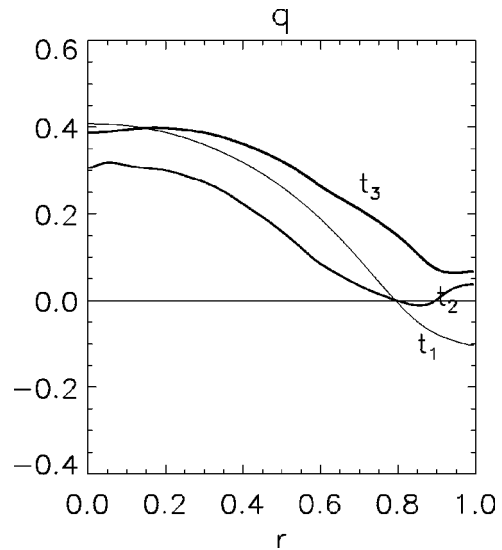


FIG. 9. The q profile at the three different times t_1 , t_2 , and t_3 for OPCD.

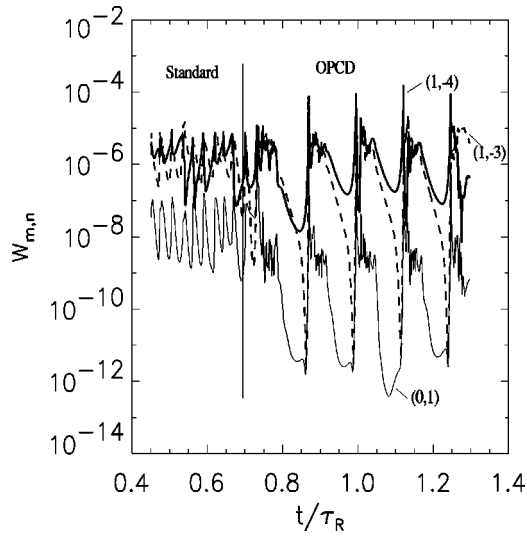


FIG. 10. Magnetic modal energy for the modes (1,-3), (1,-4), and (0,1), without (standard case) and with OPCD versus time.

(1,-2) and the $m=0$ mode (0,1) are shown in Fig. 13. Similar to OPCD, the time-averaged magnetic fluctuation level does not change significantly, but the time variations of the total magnetic fluctuations are larger than for OPCD. Large modulation amplitudes of the axisymmetric fields and q on axis cause the core mode (1,-2) to become resonant comparable in amplitude to the dominant core modes [(1,-3) and (1,-4)]. The terms in parallel Ohm's law are shown in Fig. 14 at the four different times marked in Fig. 12. At time t_1 , v_z and F are positive yielding a positive parallel electric field everywhere ($E_{\parallel} = E_z \cdot B_z > 0, E_{\theta} \sim 0$). At this time core dominant modes [(1,-3), (1,-4)] have small amplitudes (as seen in Fig. 13) and the fluctuation induced dynamo term is zero, so that $E_{\parallel} = \eta J_{\parallel}$ [Fig. 14(a)]. The core modal energies shown in Fig. 13 start to grow as E_{\parallel} becomes negative near the edge and the fluctuation amplitudes reach their largest level. The current density gradient increases as seen in Fig. 14(b). At time t_2 , E_{\parallel} becomes negative near the edge and the dynamo term becomes large to relax the current profile toward a flatter profile by suppressing the current in the core and driving current at the edge, as seen in Fig. 14(b). Field reversal is maintained as the tearing fluctuations increase and energy is transferred to the small-scale fluctuations and the $m=0$ modes grow through nonlinear mode coupling (Fig. 13).

During the second part of the phase when v_z is negative,

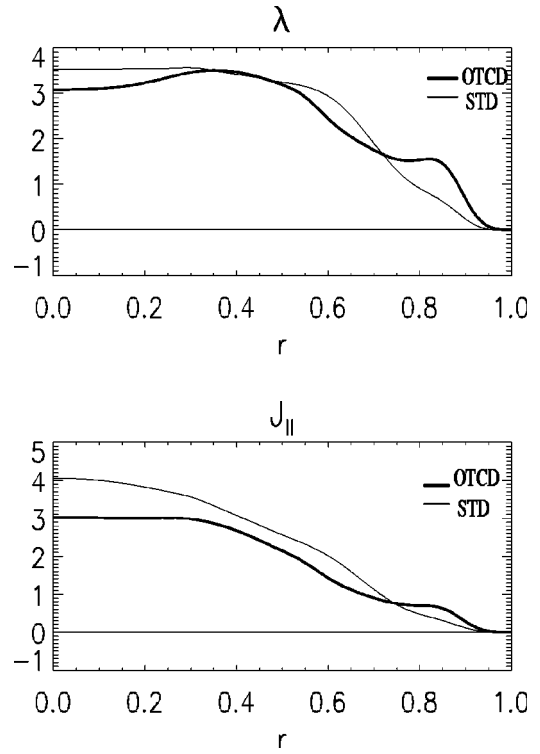


FIG. 11. Time-averaged $\lambda(r)$ and J_{\parallel} profiles shown for OTCD and standard (STD) cases.

the parallel electric field $E_{\parallel} = E_z \cdot B_z$ can become positive again since F is negative. The positive parallel electric field at time t_3 is shown in Fig. 14(c). The core tearing mode amplitudes decrease at t_3 as seen in Fig. 13 and the dynamo term is weaker due to the positive edge E_{\parallel} . As the axial electric field reaches its minimum negative value, the field reversal becomes positive yielding a negative parallel electric field near the plasma edge as shown in Fig. 14(d). The dynamo term becomes strong again to relax the current density. As is seen in Fig. 14(d), the current density in the core is fairly flat which causes the reduction of core tearing modes at later times when E_{\parallel} begins to become positive again near the edge. The cycle repeats and returns back to the profiles shown at time t_1 .

Thus, the current density profile is strongly modified, and varies significantly in time. During part of the OTCD cycle, a positive E_{\parallel} profile is generated and an edge current is driven. OTCD also flattens the current density profile in the core out to the radius $r=0.9$. The latter effect is not produced by OPCD.

TABLE I. Time-averaged quantities.

	$\overline{B/B_0}$ (%)	\overline{K}	\overline{K}_{diss}	$\overline{I_z}$	$\frac{\overline{\hat{I}_z}}{2I_z}$ (%)	\overline{F}	F_{p-p}
OPCD	1.23	6.6	47.4	2.84	8	-0.12	0.9 ($F_{\min} = -0.7, F_{\max} = 0.2$)
OTCD	1.1	5.1	40.6	2.3	60	0.0	2.0 ($F_{\min} = -1., F_{\max} = 1.$)
OFCD	0.6	8.6	72	3.0	45	-0.31	2.0 ($F_{\min} = -1.5, F_{\max} = 0.5$)
Standard	1.25	5.71	41	2.6	...	-0.12	0.17 ($F_{\min} \approx -0.2, F_{\max} \approx 0.03$)

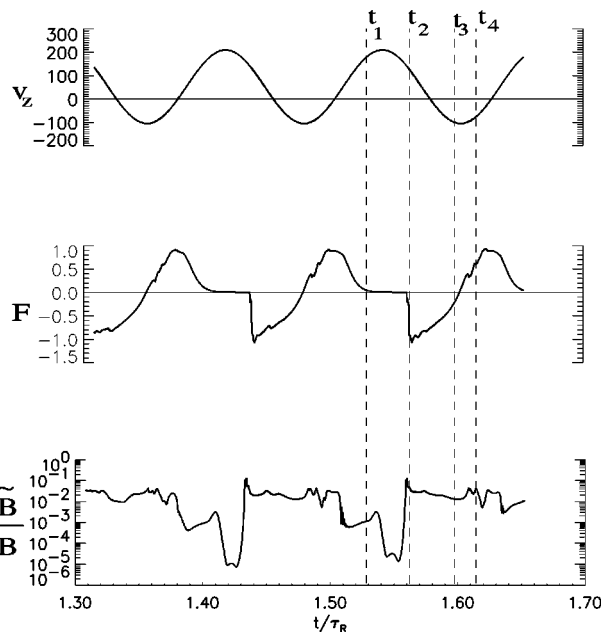


FIG. 12. The oscillating toroidal loop voltage v_z , field reversal parameter F and total magnetic fluctuations \tilde{B}/B versus time. The period of the toroidal electric field is $\tau_\omega = 0.126\tau_R$.

C. The combination of the oscillating fields—OFCD

Through the separation of oscillating poloidal field and oscillating toroidal field, we learned that the time-averaged magnetic fluctuation level remains unchanged in both cases, and the parallel electric field tends to modify the current density profile toward a more stable profile (when $E_{\parallel} > 0$) or toward a more unstable profile (when $E_{\parallel} < 0$). However, in OFCD by oscillating both poloidal and toroidal electric fields out of phase, the time-averaged magnetic fluctuations are reduced; in addition, a time-averaged magnetic helicity is injected and partial current can be maintained as shown in Sec. III (Fig. 1). Thus, the net effect requires the combination of the two oscillating fields. Here, we study the OFCD dy-

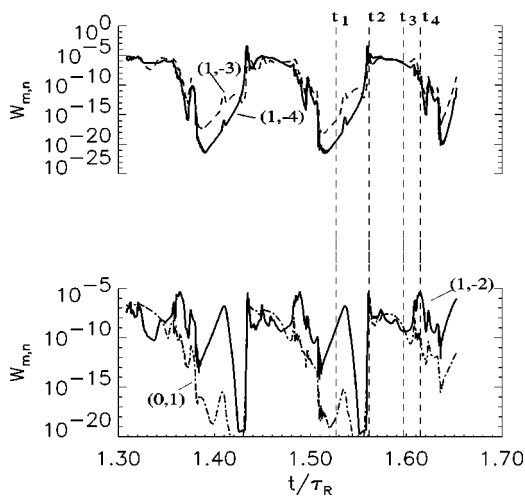


FIG. 13. The modal magnetic energy W_{mn} for (a) (1,-3), (1,-4), and (b) (0,1), (1,-2) for OTCD.

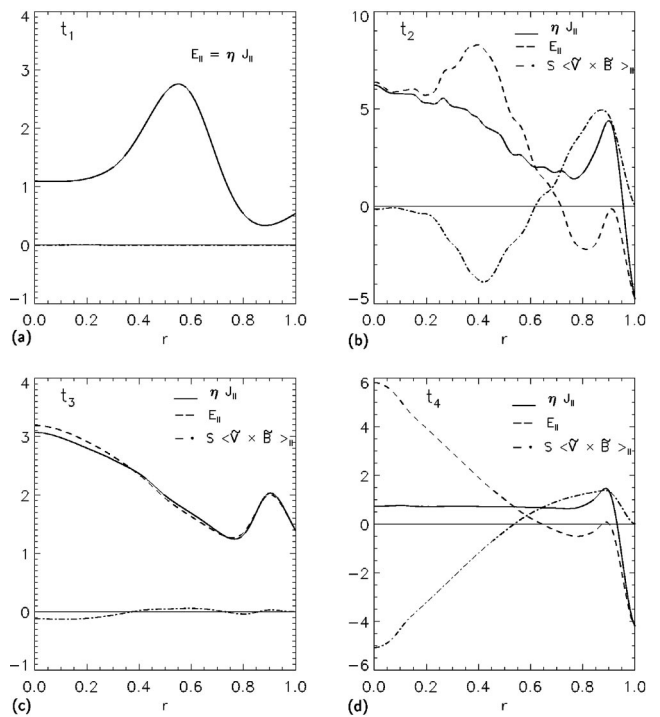


FIG. 14. The three terms $\eta J_{\parallel}, E_{\parallel}, S\langle\tilde{V}\times\tilde{B}\rangle_{\parallel}$ in parallel Ohm's law at times t_1-t_4 during a cycle for OTCD.

namics during a cycle, i.e., the effect of the oscillating fields on the axisymmetric profiles and asymmetric fluctuations.

The toroidal and poloidal loop voltages v_z and v_p , field reversal parameter F , and the total magnetic fluctuation \tilde{B}/B are shown in Fig. 15. The variations of current profile and dynamo term with regard to parallel electric field are studied

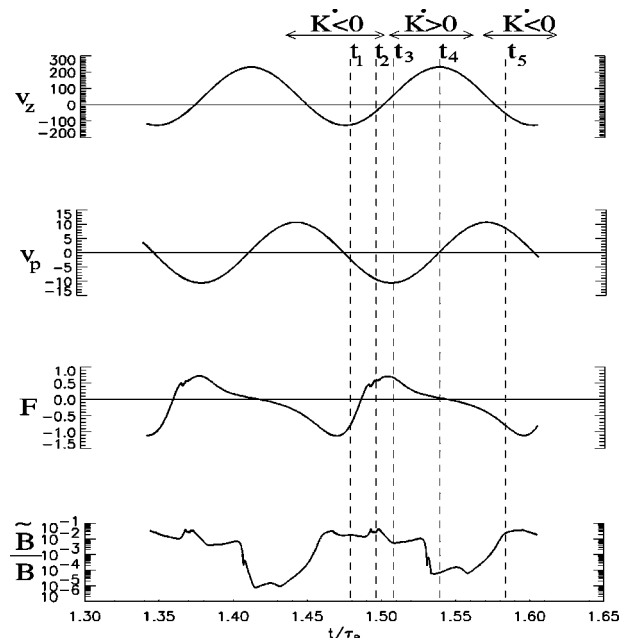


FIG. 15. The toroidal oscillating loop voltage v_z , the poloidal oscillating voltage v_p , field reversal parameter F , and the total magnetic fluctuation \tilde{B}/B versus time.

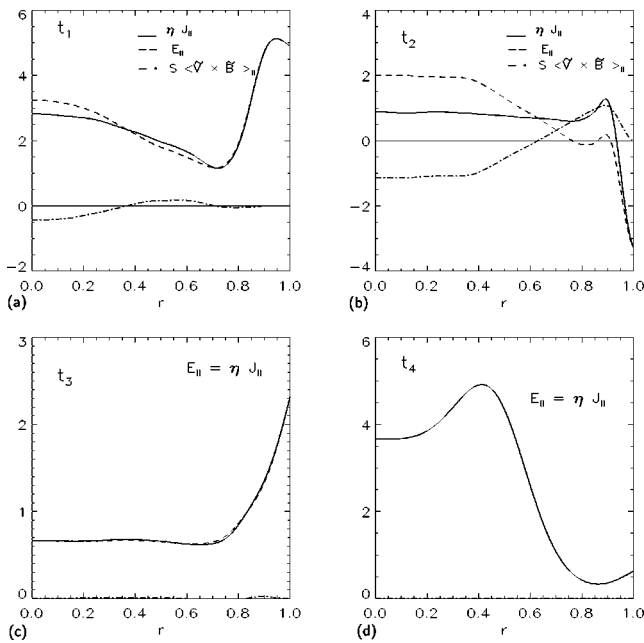


FIG. 16. The three terms E_{\parallel} , ηJ_{\parallel} and $S\langle\bar{V}\times\bar{B}\rangle$ in parallel Ohm's law at different times during an OFCD cycle marked in Fig. 15.

during a cycle. The three terms in parallel Ohm's law are shown in Fig. 16 at different times marked in Fig. 15. Because v_z and F are both negative, the parallel electric field E_{\parallel} is positive over the entire radius at time t_1 as shown in Fig. 16(a). As is seen, an edge current is driven by E_{\parallel} , and the core current density is still fairly peaked even though it is partially suppressed by the dynamo term. The magnetic fluctuation level at this time is about the same as standard plasma without OFCD. As the toroidal field loses reversal ($F>0, v_z<0$ and $v_p<0$), the parallel electric field ($E_{\parallel}=E_z\cdot B_z+E_{\theta}\cdot B_{\theta}$) becomes negative near the edge, as shown in Fig. 16(b). This causes the magnetic fluctuations to increase as seen in Fig. 15 at time t_2 . The dynamo term tends to relax the current density profile by suppressing the current in the core and driving current near the edge. The current density profile is flat in most of the core region. This current flattening in the core reduces mode growth, and causes the core resonant mode amplitudes to reduce at a later time when a positive E_{\parallel} is generated as the axial voltage v_z becomes positive (Fig. 15 at t_3). The positive parallel electric field is shown in Fig. 16(c) at t_3 . The dynamo term at this time is zero and $E_{\parallel}=\eta J_{\parallel}$. The current density on axis increases as helicity is injected into the plasma as shown in Fig. 16(d) at time t_4 (E_{\parallel} increases and $\dot{K}>0$). The current density starts to peak in the core and the core tearing modes start to grow again as seen in Fig. 15 at t_5 and the cycle repeats.

Two phases during a cycle can be distinguished, injection and ejection. During the ejection phase, the helicity injection rate is negative ($\dot{K}<0$) and the total axial current decreases (t_1, t_2 and t_5 in Fig. 15). The magnetic fluctuation amplitudes are about equal to or slightly higher than the standard (without OFCD) fluctuations in this phase. Oscillating fields flatten the current density in the core and the fluctuation level starts to decrease toward zero during the second

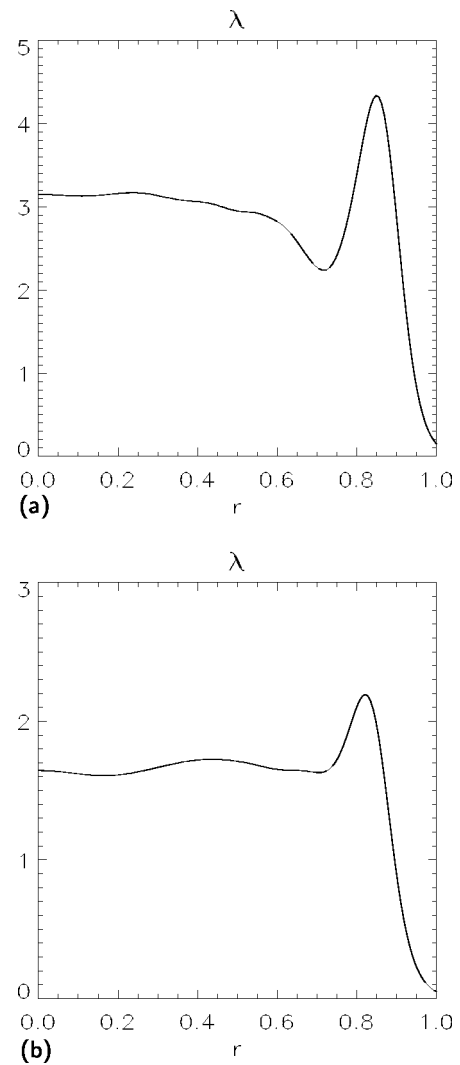


FIG. 17. The $\lambda=J_{\parallel}/B$ profiles at times (a) t_1 and (b) t_3 .

part of the cycle, the injection phase. The helicity injection rate is positive ($\dot{K}>0$) and the total axial current increases (t_3, t_4 in Fig. 15). The current profile is mainly sustained by positive E_{\parallel} in the injection phase. However, during the ejection phase, the gradient in the parallel current density profile drives the tearing instabilities. The fluctuation induced tearing dynamo term is negative in the core, suppressing the current. Therefore, both the tearing dynamo and the parallel electric field shape the λ profile. Figure 17 shows the modification of the $\lambda(r)$ profile at t_1 (during the ejection phase) and t_3 (during the injection phase). The current density is hollow near the edge at t_1 and is flattened at t_3 . The gradient of these profiles changes during a cycle. For example, during the injection phase (after t_3) the current on axis increases and the λ profile peaks. However, these λ profiles are snapshots taken at the time when the OFCD current profile modification, including current flattening in the core, is maximal.

To complete the analysis of the OFCD cycle, we examine the modal activities based on the resonant condition on the q profile. As shown before, the time-averaged magnetic fluctuations are reduced by OFCD. In Fig. 18 the effect of oscillating fields on the mode amplitudes can be seen. The

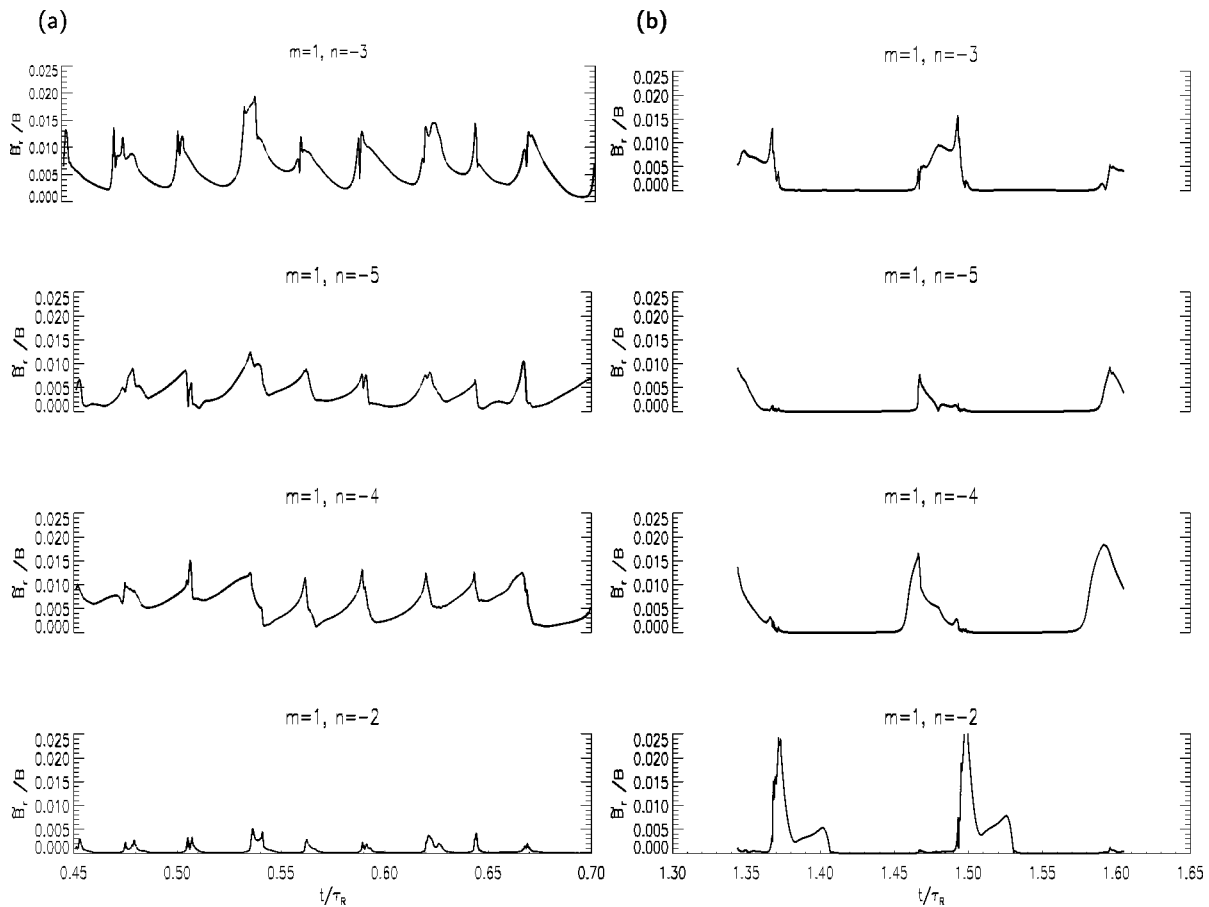


FIG. 18. The volume-averaged mode amplitudes for (a) standard case (without OFCD) and (b) with OFCD.

volume-averaged modal magnetic amplitudes ($\bar{B}_{r,m,n}/B$) for the dominant modes is zero during part of the OFCD cycle and is comparable to the standard mode amplitudes during the other part of the cycle. The mode amplitudes for the standard case without OFCD are shown for comparison. The dominant modes without OFCD are (1, -3), (1, -4). Because of the large variation of the axisymmetric profiles with OFCD another core mode (1, -2) reaches an amplitude comparable to the core modes without OFCD.

The magnetic modal activity changes significantly with the q profile variations during an OFCD cycle. Figure 19 shows the q profiles at times t_1-t_4 . The q profile at time t_1 is for the standard RFP. At time t_2 the q profile is positive everywhere and the $m=1, n=-2$ and $m=1, n=-3$ core modes are dominant (Fig. 18). At a later time (t_3) the mode amplitudes of (1, -3) and (1, -4) are suppressed and the $m=1, n=-2$ mode is resonant (Fig. 19). The q profile on axis drops again at a later time t_4 . The core mode (1, -4) grows linearly when the current density profile peaks in the core at the time the total fluctuation level is minimum. This linear growth is seen in the total magnetic fluctuations \bar{B}/B (Fig. 15 at time t_5) and in the mode amplitude of (1, -4) shown in Fig. 18. Thus a single helicity state is formed (after t_4). The single helicity mode grows until it reaches an amplitude high enough to cause nonlinear coupling. The field line trajectory during the single helicity state is shown in Fig. 20(c). Because of the nonlinear coupling of this mode with

other modes and a cascading process, the magnetic energy spectrum becomes broad again. The stochasticity of the magnetic field lines increases to the level of the standard RFP shown in Fig. 20(a). As is seen in Fig. 20, there is a transition

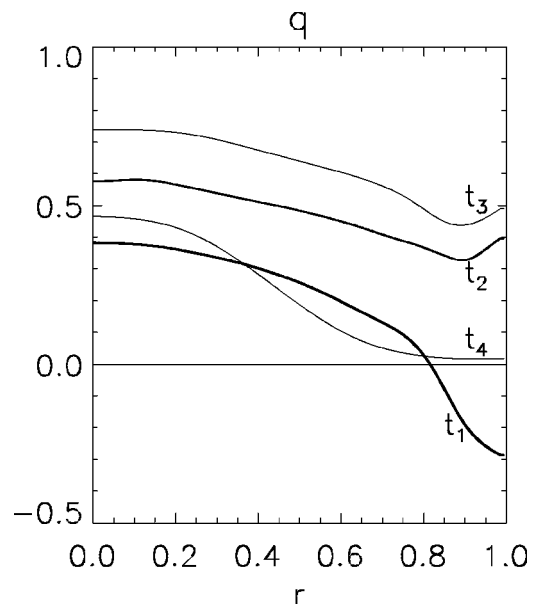


FIG. 19. The q profiles at times t_1-t_4 .

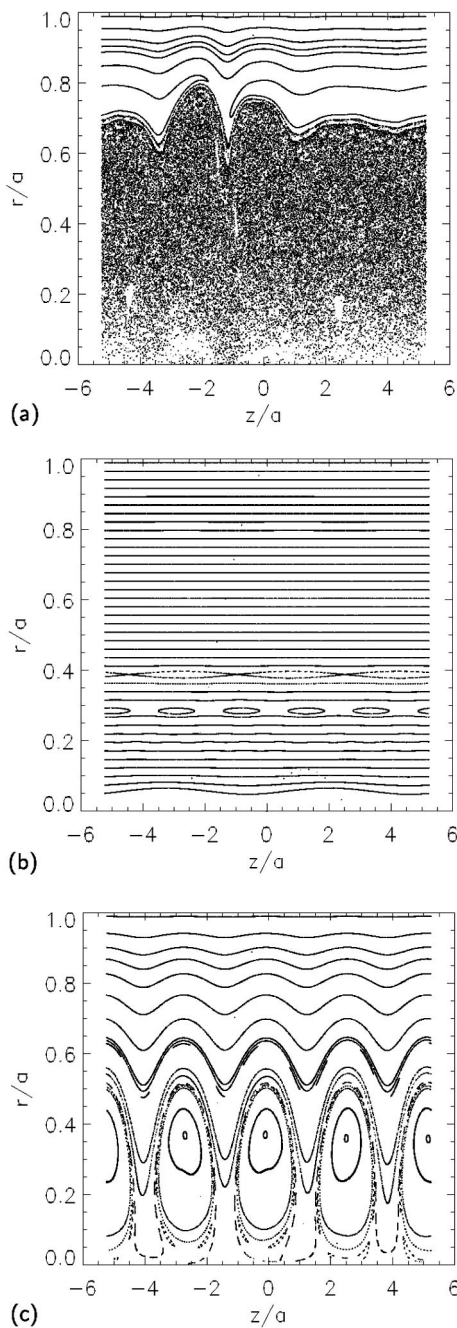


FIG. 20. Field line trajectory (Poincare plots) at times (a) t_1 , (b) t_4 , and (c) t_5 .

from stochastic magnetic field lines to ordered and then to the single helicity state.

A key feature of OFCD is that E_{\parallel} remains positive for most ($\sim \frac{3}{4}$) of the OFCD cycle. This is in contrast to OPCD and OTCD in which $E_{\parallel} < 0$ near the edge for almost half of the cycle. Hence, OFCD is more effective.

In summary, the current profile is altered significantly during an OFCD cycle. During the ejection phase the current profile is peaked in the core and has a hollow shape closer to the edge because of the oscillations of the OFCD-driven current near the edge region. During this phase the tearing dynamo term distributes the current density by suppressing the

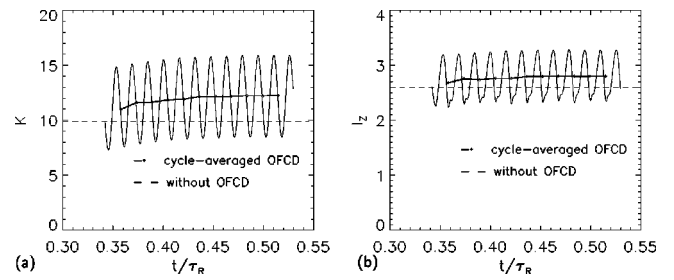


FIG. 21. (a) The magnetic helicity and (b) total axial current at the frequency $\omega\tau_H = 1.2$.

current in the core and driving current near the edge. The q profile and the modal activity are also similar to the standard RFP. As the total current decreases, the parallel electric field is modified in the core and also becomes positive near the edge. As a result, the current density is relaxed to a flat profile. The flattening of the current density profile results in nearly complete suppression of the magnetic fluctuations and the tearing dynamo term vanishes. The cycle repeats when the current profile peaks.

V. THE FREQUENCY DEPENDENCE

OFCD depends on the ac helicity injection rate which is proportional to the ratio of the ac driving voltages and the oscillation frequency. The penetration of the OFCD-driven current into the plasma and the OFCD modification of the current density profile also depends upon the frequency. As mentioned before, the oscillation frequency should be low enough for sufficient current relaxation by the tearing fluctuations, but high enough to avoid current reversal. The frequency should be selected to result in a flattening of the current profile by the oscillating fields. Here, the results of 3-D MHD computations at different OFCD frequencies are presented when the helicity injection rate is fixed.

Oscillating fields with frequencies $\omega\tau_H = 1.2$, $\omega\tau_H = 4.7$, and $\omega\tau_H = 9.8$ are imposed on a relaxed RFP at aspect ratio $R/a = 2.88$. The oscillating field with the frequency $\omega\tau_H = 1.6$ (discussed in the previous section) and $\omega\tau_H = 0.8$ are also imposed on a target plasma with the same current but with the aspect ratio $R/a = 1.66$. Figure 21(a) shows that the oscillating fields inject helicity into the standard RFP plasma at time $t = 0.34 \tau_R$ with frequency $\omega\tau_H = 1.2$ and with the helicity injection rate of 50% of the ohmic helicity rate ($\dot{K}_{inj} = \hat{v}_z \hat{v}_{\theta} / 2\omega = 40$). As shown in Fig. 21(b), total axial current is increased by 10%. The peak to peak current modulation amplitude is about 35% of the mean total axial current and it is much smaller than the modulation amplitudes shown in Fig. 1 at $\omega\tau_H = 0.16$. The mean helicity dissipation rate, $\dot{K}_{diss} = \eta \int J \cdot B dV$, is increased with OFCD (Fig. 22) and balances the total helicity injection rate (ac and ohmic injection) as the plasma gets close to steady-state. However, the fluctuating helicity dissipation rate, $\eta \int \tilde{J} \cdot \tilde{B} dV$, remains small (similar to the standard RFP surrounded by a conducting wall).

Table II summarizes the results of the OFCD simulations with the same helicity injection rate but with different fre-

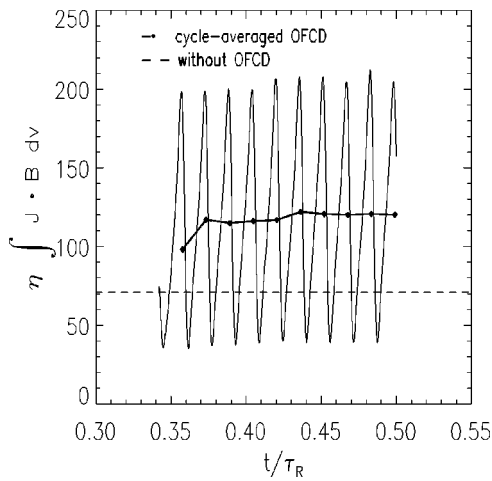


FIG. 22. The helicity dissipation rate $\dot{K}_{diss} = \eta \int J \cdot B$ versus time. The total helicity dissipation rate is balanced by the helicity injection rate as the plasma gets close to steady-state at time $t = 0.5 \tau_R$. The fluctuating helicity dissipation rate is almost zero.

quencies. The current modulation amplitudes $\hat{I}_z/2I_z$ and the peak-to-peak modulation of the field reversal parameter F_{p-p} are reduced at higher frequency. The reduction of the modulation amplitudes with frequency obtained here is consistent with the results from the linear 1-D calculations and the relaxed-state scaling of full current sustainment by OFCD.⁴ However, a similar frequency-scaling study using numerically demanding 3-D computations would require more data points than what is currently feasible. The time-averaged total magnetic fluctuations \bar{B}/B_0 are suppressed by a factor of 2 at $\omega\tau_H = 0.16$ as shown in Sec. III. However, \bar{B}/B_0 is about the same as the standard fluctuation level at higher OFCD frequency (see Table II).

The cycle-averaged symmetric OFCD-driven dynamo term $(V_{00} \times B_{00})_{\parallel}$, a main determinant of the λ profile, is shown in Fig. 23 for different frequencies. The classical penetration [$\delta = (\eta/\omega)^{1/2}$] for a fixed helicity input rate increases with the OFCD period. At lower frequency, $\omega\tau_H \sim 1$, the OFCD-driven current penetration is deeper into the plasma. Figure 24 shows the cycle-averaged current density profile for different frequencies. The ohmic current density profile is modified by OFCD. At higher frequencies, $\omega\tau_H \gg 1$, the OFCD-driven current is mostly peaked near the plasma edge, but at lower frequency ($\omega\tau_H \sim 1$) the OFCD-

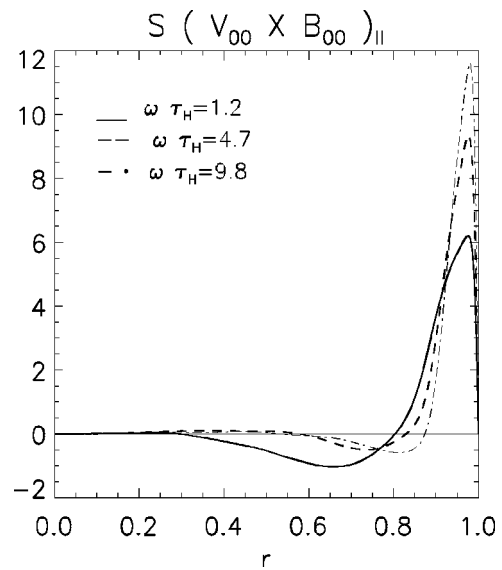


FIG. 23. The cycle-averaged axisymmetric dynamo-like term, $(V_{00} \times B_{00})_{\parallel}$, for partial OFCD sustainment at three different frequencies.

driven current is further into the plasma. At $\omega\tau_H = 1.2$, J_{\parallel} is increased everywhere, but mainly near the edge region. We also note that there is an exponentially growing resistivity profile near the plasma edge which causes current dissipation near the plasma edge at high frequencies ($\omega\tau_H \gg 1$).

Figure 25 illustrates the temporal variation of $\lambda(r)$ profiles with oscillating fields for frequencies $\omega\tau_H \sim 1$ and $\omega\tau_H \gg 1$. As is seen the OFCD-driven current is more localized near the edge region for $\omega\tau_H \gg 1$. The modifications of the time-averaged $\lambda(r)$ and q profiles with OFCD at frequencies $\omega\tau_H \leq 1$ are shown in Fig. 26. The current density gradient between $r = 0.4$ and $r = 0.8$ is smaller in the $\omega\tau_H = 0.16$ case leading to a lower time-averaged magnetic fluctuation level. The field reversal modulations are higher at lower frequencies (Table II) and field reversal is lost during part of the cycle. Thus, the time-averaged q at the edge is smaller for $\omega\tau_H = 0.16$ than for $\omega\tau_H = 0.8$ as shown in Fig. 26(b).

VI. CONCLUSIONS

We have examined current profile control by OFCD using 3-D MHD computation. We find that OFCD can control the current density profile in an oscillatory steady-state, lead-

TABLE II. OFCD simulation results for different frequencies.

		\bar{B}/B_0 (%)	\bar{K}	\bar{K}_{diss}	\bar{I}_z	$\frac{\hat{I}_z}{2I_z}$ (%)	F_{p-p}
Case I	Standard (R/a=1.66)	1.25	5.71	41	2.6	...	0.17
	$\omega\tau_H = 0.16$	0.6	8.6	72	3.0	45	2.0
	$\omega\tau_H = 0.8$	1.5	7.3	71	2.82	21	1.58
Case II	Standard (R/a=2.88)	1.27	9.8	70	2.6	...	0.09
	$\omega\tau_H = 1.2$	1.0	12.2	120	2.8	16	1.4
	$\omega\tau_H = 4.7$	1.44	10.2	112	2.6	11	0.95
	$\omega\tau_H = 9.8$	1.46	9.8	111	2.6	8	0.9

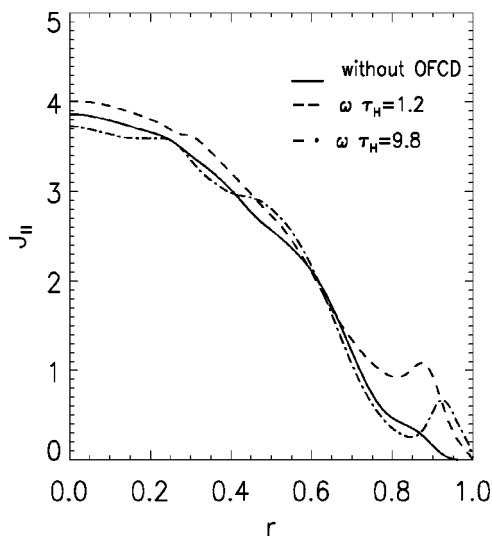


FIG. 24. The cycle-averaged parallel current density profiles of standard RFP (solid), OFCD with the frequency $\omega\tau_H \sim 1$ (dashed), and OFCD with the high frequency $\omega\tau_H \gg 1$ (dash-dotted).

ing to a significant reduction in magnetic fluctuations. The detailed dynamics of OFCD is quite complex, owing to the strong time variation of all key quantities, both mean and fluctuating. Thus, to elucidate the key ingredients needed for the fluctuation reduction, we separately examine the imposition of an oscillating poloidal electric field only (OPCD) and the imposition of an oscillating toroidal electric field only (OTCD).

We find that neither OPCD nor OTCD leads to a reduction in the time-averaged magnetic fluctuation amplitude. The current density profile is more stable during the phase when the parallel electric in the edge is positive, and less stable when the parallel electric field is negative, leading to a net effect that is small. However, when both surface voltages are oscillated simultaneously, but out of phase, the parallel electric field is maintained positive over a majority of the

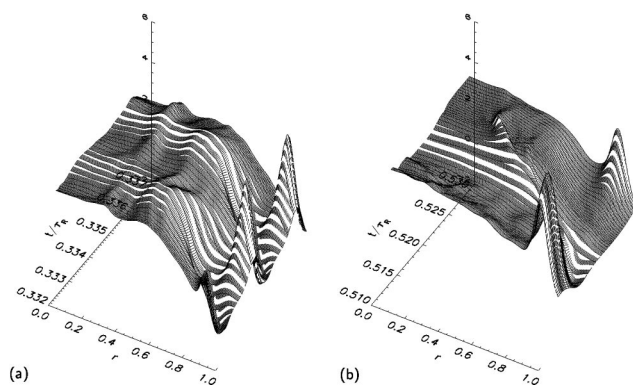


FIG. 25. The $\lambda(r)$ profile versus time (a) $\omega\tau_H = 9.8$ and (b) $\omega\tau_H = 1.2$.

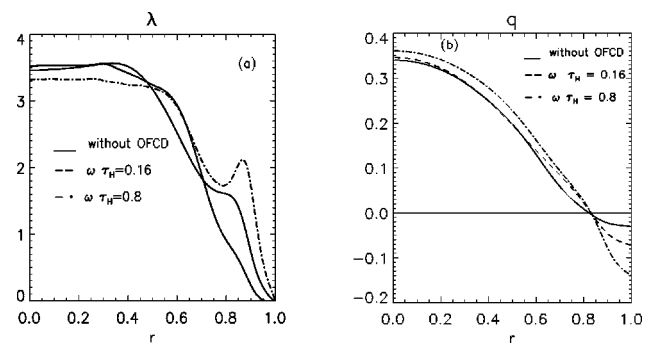


FIG. 26. The cycle-averaged (a) $\lambda(r)$ profile and (b) q profile for standard case and OFCD with $\omega\tau_H \lesssim 1$.

cycle. Hence, the time-averaged magnetic fluctuations are halved. During about half of the cycle the fluctuations are comparable to that in a standard RFP plasma, while during the other half the fluctuations are negligible. Moreover, when the fluctuations are large, part of the time one mode dominates and closed magnetic helical surfaces form. Thus, the magnetic surface are nonstochastic for much of the cycle. The two phases of the cycle correspond roughly to helicity ejection, during which the current density profile peaks and fluctuations grow, and helicity injection during which the process reverses.

OFCD current profile control also injects magnetic helicity over a cycle and sustains a portion of the total plasma current. An optimum period is found for fluctuation reduction, residing between the reconnection time and the resistive diffusion time. The time-varying nature of the resulting confinement might present some practical difficulties for a reactor or long-pulse experiment, but the steady-state aspect of the technique might provide an advantage over transient inductive techniques employed in present experiments.

ACKNOWLEDGMENTS

We thank John Sarff and Karsten McCollam for useful discussions.

- ¹J. S. Sarff, S. A. Hokin, H. Ji, S. C. Prager, and C. R. Sovinec, *Phys. Rev. Lett.* **72**, 3670 (1994).
- ²B. E. Chapman, A. F. Almagri, J. K. Anderson *et al.*, *Phys. Plasmas* **9**, 2061 (2002); B. E. Chapman, J. K. Anderson, T. M. Biewer *et al.*, *Phys. Rev. Lett.* **87**, 205001-1 (2001).
- ³M. K. Bevir and J. W. Gray, in *Proceedings of the Reversed-Field Pinch Theory Workshop*, edited by H. R. Lewis and R. A. Gerwin (Los Alamos Scientific Laboratory, Los Alamos, NM, 1981), Vol. III, p. A-3.
- ⁴F. Ebrahimi, S. C. Prager, J. S. Sarff, and J. C. Wright, *Phys. Plasmas* **10**, 999 (2003).
- ⁵T. H. Jensen and M. S. Chu, *Phys. Fluids* **27**, 2881 (1984).
- ⁶M. K. Bevir, C. G. Gimblett, and G. Miller, *Phys. Fluids* **28**, 1826 (1985).
- ⁷Y. L. Ho, *Nucl. Fusion* **31**, 341 (1991).
- ⁸R. Bartiromo, V. Antoni, T. Bolzonella *et al.*, *Phys. Plasmas* **6**, 1830 (1999).
- ⁹D. D. Schnack, D. C. Barnes, Z. Mikic, D. S. Harned, and E. J. Caramana, *J. Comput. Phys.* **70**, 330 (1987).